Electronic Supplementary Material (ESI) for Soft Matter.

Supplementary Information

Anisotropy versus fluctuations in fractal self-assembly of gold nanoparticles

Anurag Singh[a], Suparna Khatun[a] and Amar Nath Gupta[a]*

[a]Biophysics and Soft Matter Laboratory, Department of Physics, IIT Kharagpur, Kharagpur-721302, India

*Corresponding author's email id: ang@phy.iitkgp.ac.in

S1. Fractal self-assembly of AuNPs formed in the absence and the presence of visible light

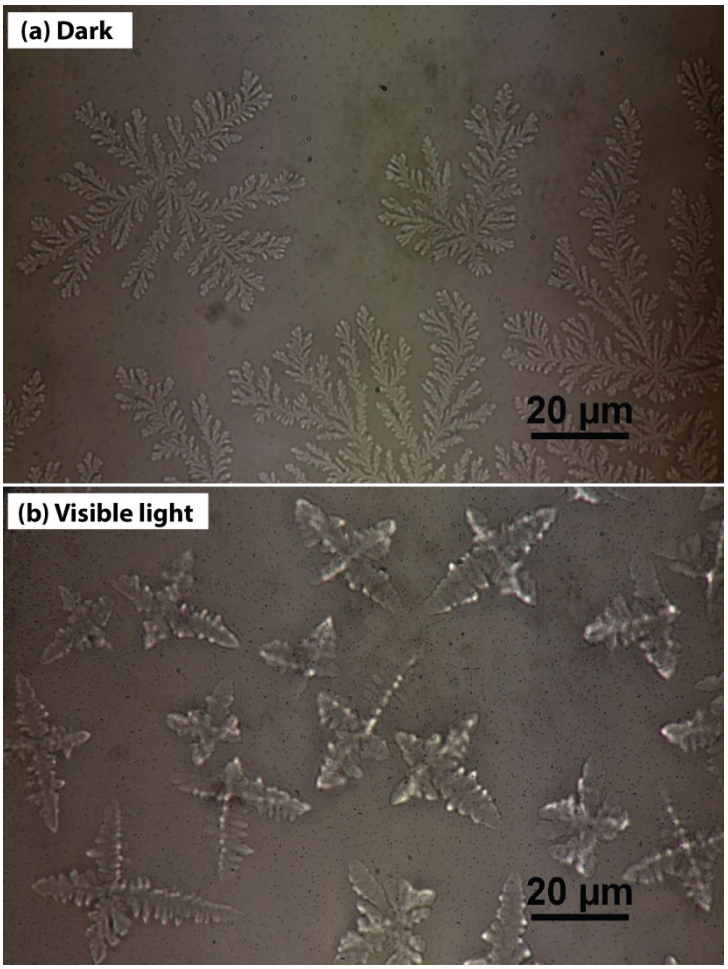

Figure. S1. Fractal self-assembly of gold nanoparticles observed from the gold colloid when air-dried in (a) dark and the (b) presence of visible light. The fractal-like and cross-shaped morphologies are visible in the figure.

S2. Evidence for fractal self-assembly of AuNPs

The fractal self-assemblies that we observed must be originated from the constituents present in the as-prepared gold nanoparticles (AuNPs), which are the sodium citrate used for stabilizing the AuNPs and the AuNPs in the as-prepared solution. To confirm that the aggregates are formed from the AuNPs, we performed control experiments with sodium citrate solution with no AuNPs in it. The morphologies obtained, with the same experimental protocol as used for the as-prepared solution, for sodium citrate is shown below (Fig. S2A). Only small salt clusters were seen indicating that sodium citrate was unable to form these morphologies itself. Therefore, the fractal morphologies that we observed were from the AuNPs present in the as-prepared solution.

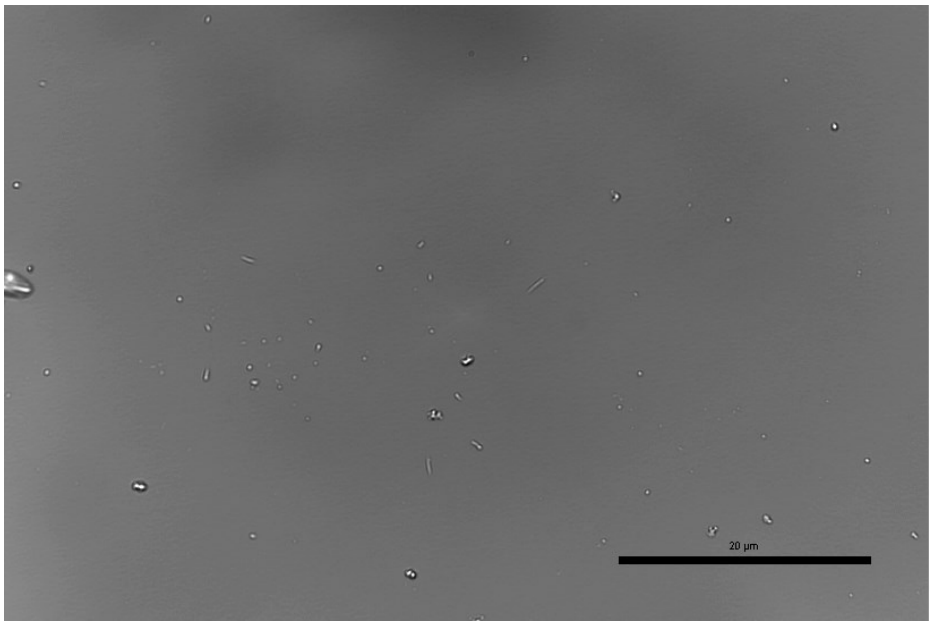

Figure. S2A. The microscopic image obtained from the control experiment performed with sodium citrate to confirm that the observed fractal morphologies were from the AuNPs. The scale bar corresponds to 20 µm.

At the beginning of the experiments, we also characterize the AuNPs, also to assure that AuNPs were present in the as-prepared solution used for the final experiments, using three different ways.

1. Surface plasmon resonance (SPR) spectra of the as-prepared solution were acquired (Fig. S2B), which showed the characteristic peak of AuNPs at 520 nm.

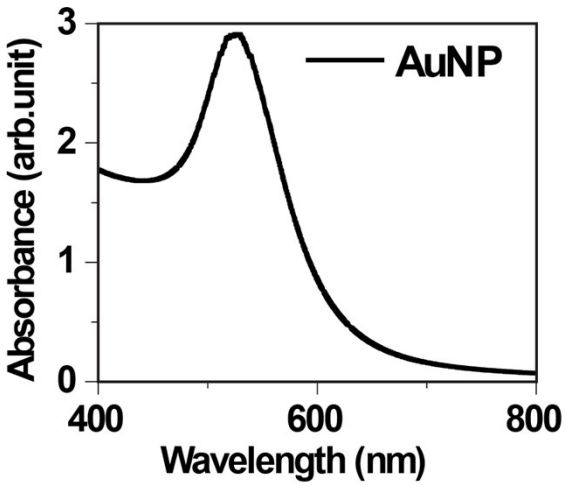

Fig. S2B. Surface plasmon resonance spectrum of as-prepared AuNPs sample.

2. The transmission electron microscopy (TEM) images of the gold nanoparticles in the as-prepared solution were taken to characterize the size distribution of the gold nanoparticles (Fig. 2 (d) in the main text).

3. The zeta potential measurements were performed to obtain the net charge on the surface of the AuNPs (using Horiba Scientific Nano Particle Analyzer SZ-100). The measurement revealed the zeta potential of -32.0±0.5 mV, which is sufficient for the gold colloid to be stable [1, 2].

Moreover, as mentioned in the main text also, we divided the solution into three parts – supernatant, intermediate, and as-prepared. The presence of AuNPs in all these three parts were confirmed using dynamic light scattering (DLS) experiments (Fig. 2(a), (b), and (c) respectively in the main text).

The modulation of these parameters (particle distribution and the net charge on the surface of AuNPs) may modulate the observed fractal self-assembly. These are precisely the subject matter of our on-going investigations.

S3. Fractal dimension

Table S3. The fractal dimension of the obtained structures $\forall\, m, \sigma \,\epsilon\, G(m;\sigma^2)$

		σ								
		0	0.5	1	1.5	2	4	6	8	10
m	1	1.62± 0.02	1.61± 0.02	1.61± 0.01	1.60± 0.01	1.60± 0.01	1.58± 0.02	1.59± 0.03	1.58± 0.02	1.59± 0.01
	2	1.62± 0.01	1.61± 0.02	1.59± 0.01	1.60± 0.01	1.59± 0.02	1.60± 0.02	1.59± 0.03	1.61± 0.02	1.58± 0.02
	3	1.59± 0.01	1.59± 0.01	1.60± 0.01	1.59± 0.01	1.59± 0.02	1.59± 0.01	1.60± 0.02	1.59± 0.01	1.59± 0.02
	4	1.58± 0.01	1.58± 0.02	1.58± 0.02	1.59± 0.02	1.59± 0.02	1.59± 0.03	1.58± 0.02	1.59± 0.03	1.59± 0.02
	5	1.57± 0.01	1.57± 0.01	1.56± 0.02	1.56± 0.02	1.59± 0.02	1.59± 0.03	1.59± 0.03	1.59± 0.01	1.59± 0.02
	6	1.57± 0.01	1.56± 0.01	1.55± 0.01	1.55± 0.01	1.58± 0.01	1.59± 0.02	1.59± 0.02	1.60± 0.02	1.59± 0.03
	7	1.56± 0.01	1.55± 0.01	1.54± 0.01	1.55± 0.03	1.55± 0.01	1.59± 0.02	1.58± 0.01	1.58± 0.03	1.59± 0.02
	8	1.56± 0.01	1.55± 0.01	1.54± 0.01	1.53± 0.01	1.54± 0.02	1.59± 0.03	1.58± 0.02	1.58± 0.02	1.57± 0.03

S4. Contour plot depicting morphological phase transition

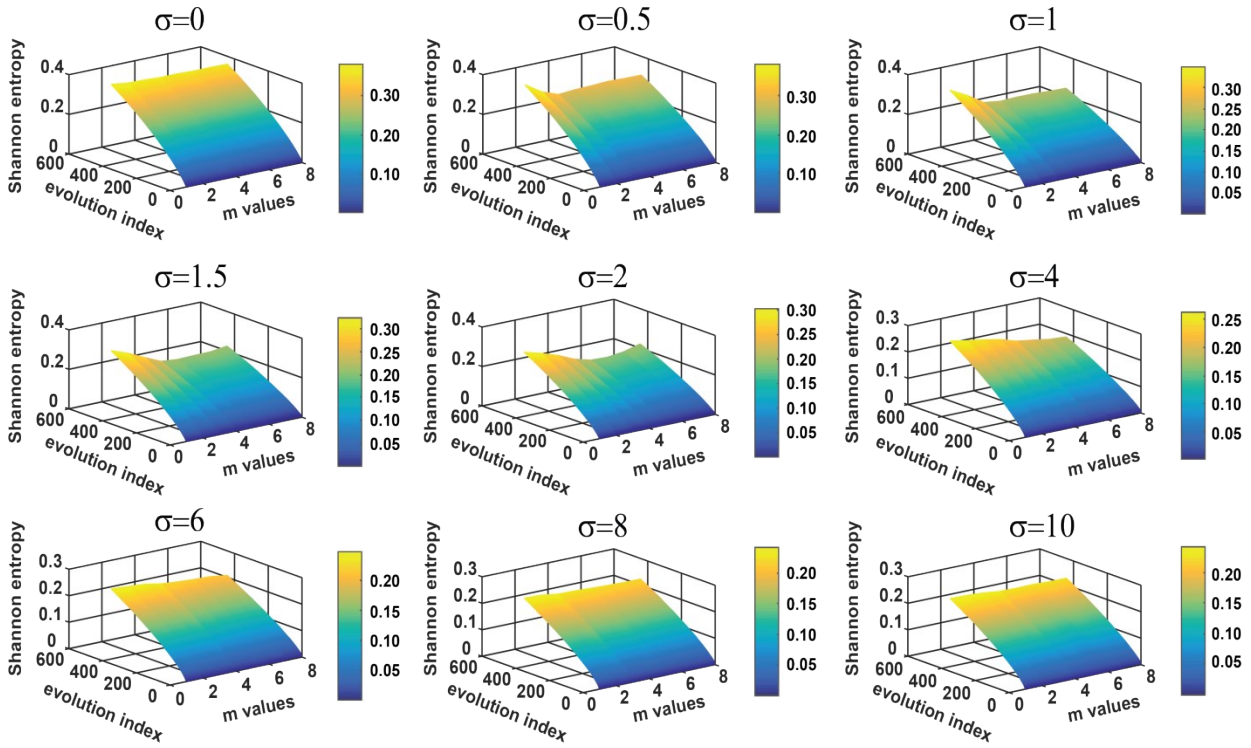

Figure S4. The 3D contour plot of the variation in the *S* values for structures obtained on the square lattice for m=1, 2,...8 drawn from $G(m,\sigma^2)$ with σ=0, 0.5, 1, 1.5, 2, 4, 6, 8 and 10. The evolution index represents the snapshot # extracted from the video of which the Shannon entropy was calculated.

S5. Interdependency plot

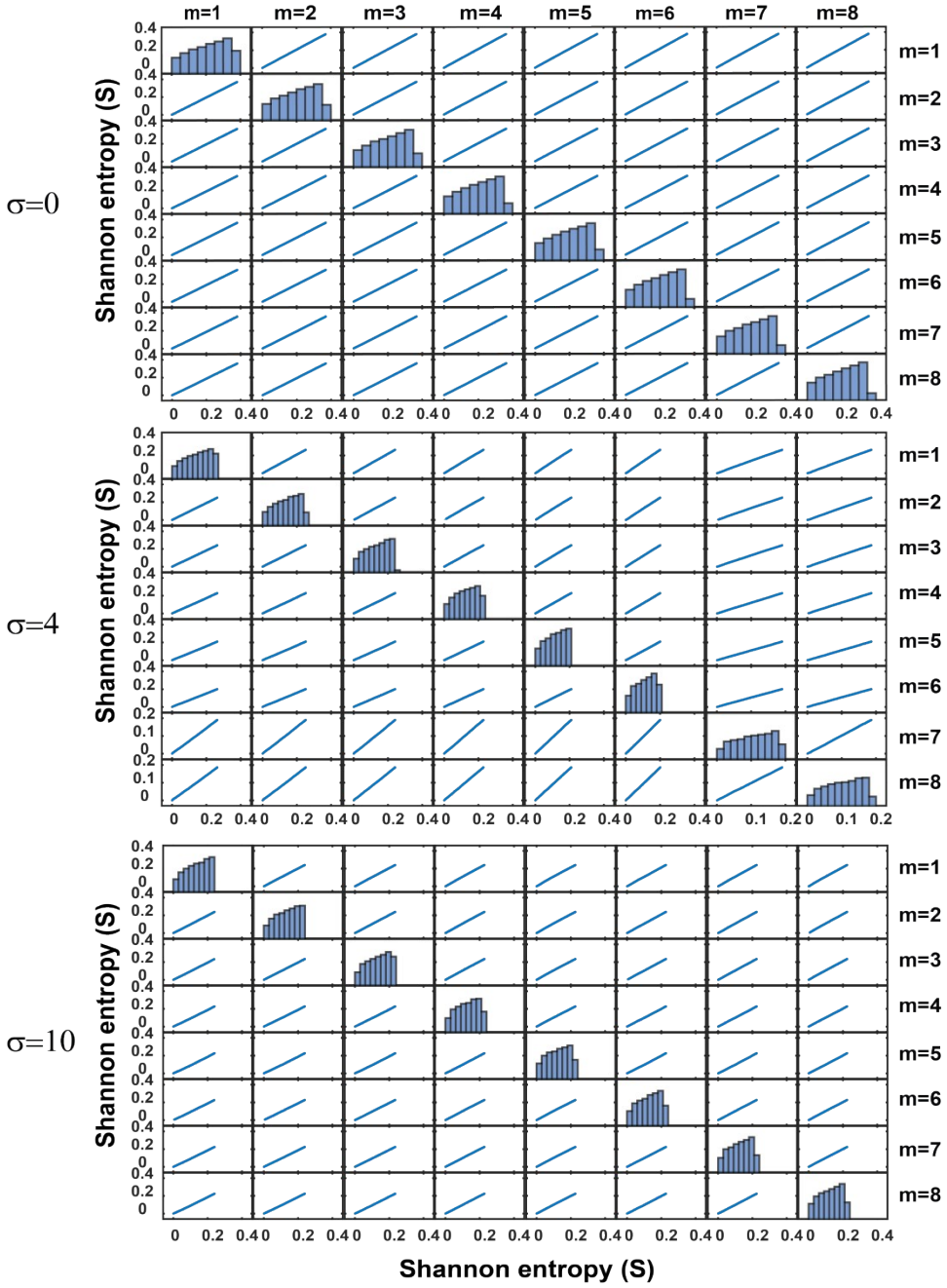

Figure S5. The s_{ij}^{k}-matrix for σ=0, 4 and 10 represents the interdependency between m_i and m_j drawn from $G(m,\sigma^2)$ with σ=0, 4, and 10, respectively. σ=0 corresponds to the growth with particles having the same p with the majority of smaller size particles. σ=4 and 10 corresponds to a system of particles having a mixture of different kind of particles having σ=4 and 10 in $G(m,\sigma^2)$. The diagonal elements represent the histogram plot of the (m_i vs. m_i) plot and the off-diagonal elements depict the correlation between m_i and m_j of the ($m_i \; vs. \; m_j$) plot.

S6. $\Delta\theta_{Int}$ Matrix with m_i as reference

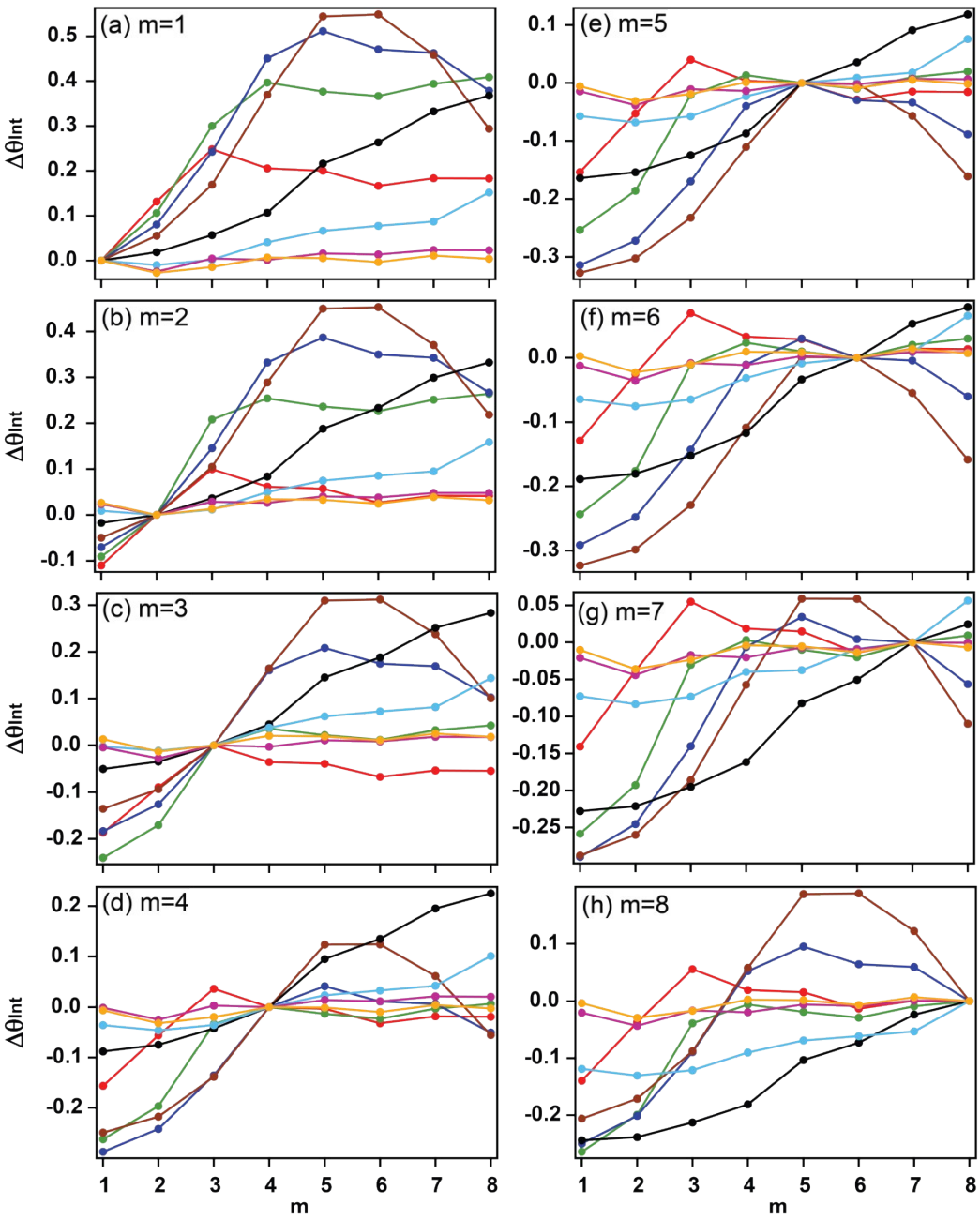

Figure S6. The comparative plot for the differences in the s_{ij}^{k} corresponding to (a) m=1, (b) m=2, (c) m=3, (d) m=4, (e) m=5, (f) m=6, (c) m=7 and (c) m=8 with reference to σ=0. All the graphs contain eight curves with reference morphologies corresponding to σ=0.5 (red), σ=1 (green), σ=1.5 (blue), σ=2 (brown), σ=4 (black), σ=6 (cyan), σ=8 (magenta) and σ=10 (orange) respectively.

S7. Quantification of morphological phase transition in Gaussian noise reduced DLA

The phase transition was quantified by fitting the variations in the δ_{ij}^{k} ($\Delta\theta_{Int}$ matrices) corresponding to (a) σ=0.5, (b) σ=1, (c) σ=1.5, (d) σ=2, (e) σ=4, (f) σ=6, (c) σ=8 and (c) σ=10 with reference to σ=0. At smaller values of σ=0.5, 1, 1.5 and 2, exponential fitting with equation $\Delta\theta_{Int=}(\Delta\theta_{Int})_{offset} + (\Delta\theta_{Int})_0 e^{-\omega m}$ was performed; power-law with equation $\Delta\theta_{Int=}(\Delta\theta_{Int})_{offset} + (\Delta\theta_{Int})_0 m^{\omega}$ for σ=4 and 6; and linear equation $\Delta\theta_{Int=}(\Delta\theta_{Int})_0 + \omega m$ was used for σ=8 and 10. The power and the linear fitting equations are the second-order and the first-order truncation of the exponential fitting equation. This indicates that with an increase in σ, the variations in δ_{ij}^{k} is feasible to be explained with the second and the first-order approximation of the fitting equation (exponential) required for capturing the variation in δ_{ij}^{k} for σ=0. The requirement of different fitting laws at different ranges of σ depicts the morphological phase transition. It is interesting to note that the fractal formation under noise fluctuations can be considered as a three-state process, with three states being the σ=0.5, 1, 1.5 and 2; σ=4 and 6; σ=8 and 10, evident by the need of different fitting laws required in the three regimes (Table S7). Our results indicate that there is a limit up to which noise reduction can be achieved, indicating that directionality is not expected after a certain level of noise in the system. The fitting parameters indicated the decrement in the rate of fitting law with errors becoming pronounced with an increase in σ (see Table S7).

Table S7. The fitting results for the differences in the δ_{ij}^{k} ($\Delta\theta_{Int}$ matrices) corresponding to (a) σ=0.5, (b) σ=1, (c) σ=1.5, (d) σ=2, (e) σ=4, (f) σ=6, (c) σ=8 and (c) σ=10 with reference to σ=0.

	Fitting equations		
	$\Delta\theta_{Int=}(\Delta\theta_{Int})_{offset} + (\Delta\theta_{Int})_0 e^{-\omega m}$	$\Delta\theta_{Int=}(\Delta\theta_{Int})_{offset} + (\Delta\theta_{Int})_0 m^{\omega}$	$\Delta\theta_{Int=}(\Delta\theta_{Int})_0 + \omega m$
σ	ω	ω	ω
0.5	1.59±0.88	-	-
1	0.57±0.16	-	-
1.5	0.50±0.24	-	-
2	0.43±0.35	-	-
4	-	1.32±0.26	-
6	-	1.87±0.55	-

8	-	-	0.005±0.001
10	-	-	0.003±0.001

S8. Experimental images for the proposed model

(a)

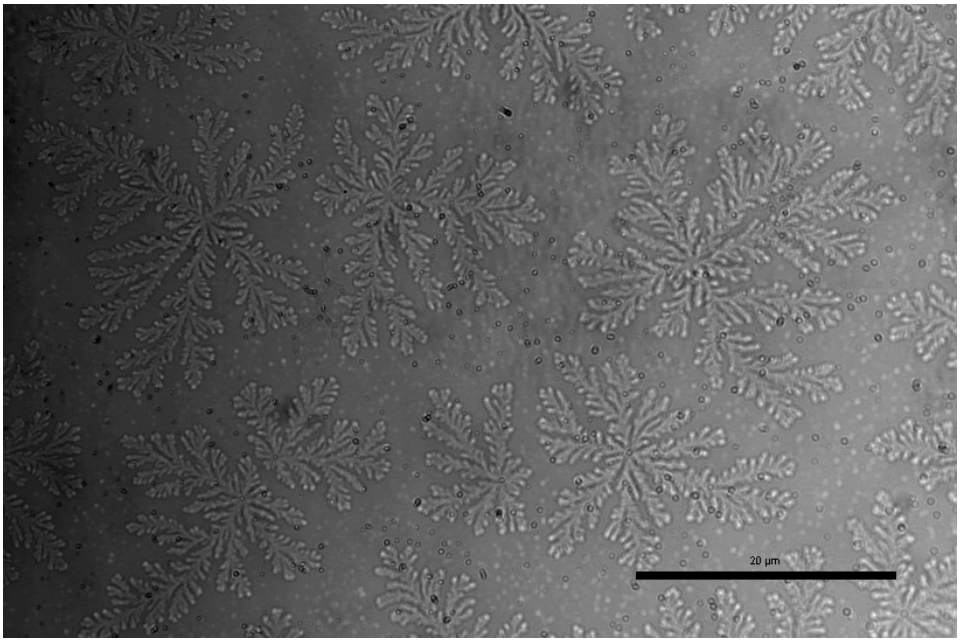

(b)

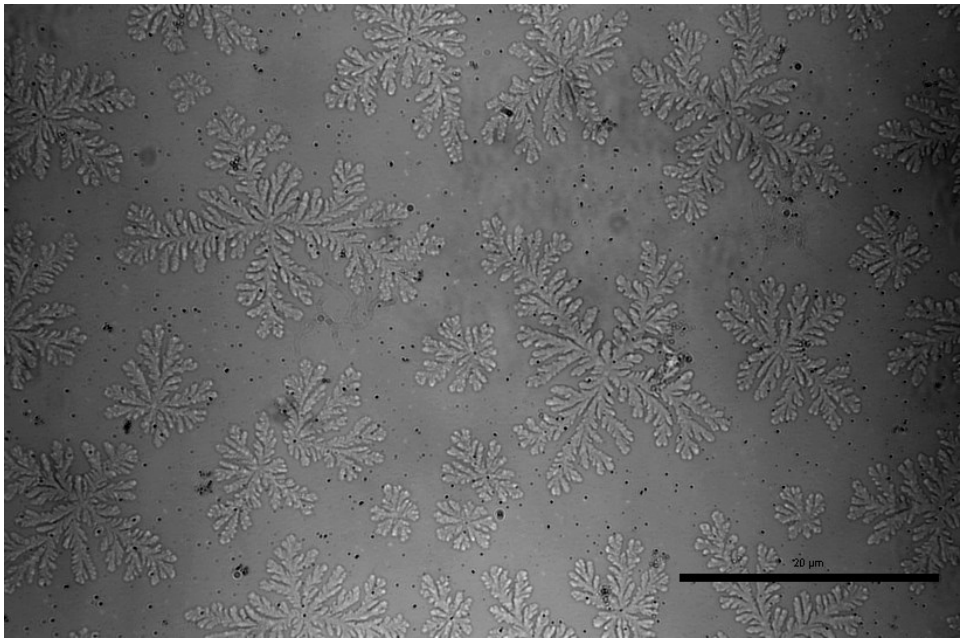

(c)

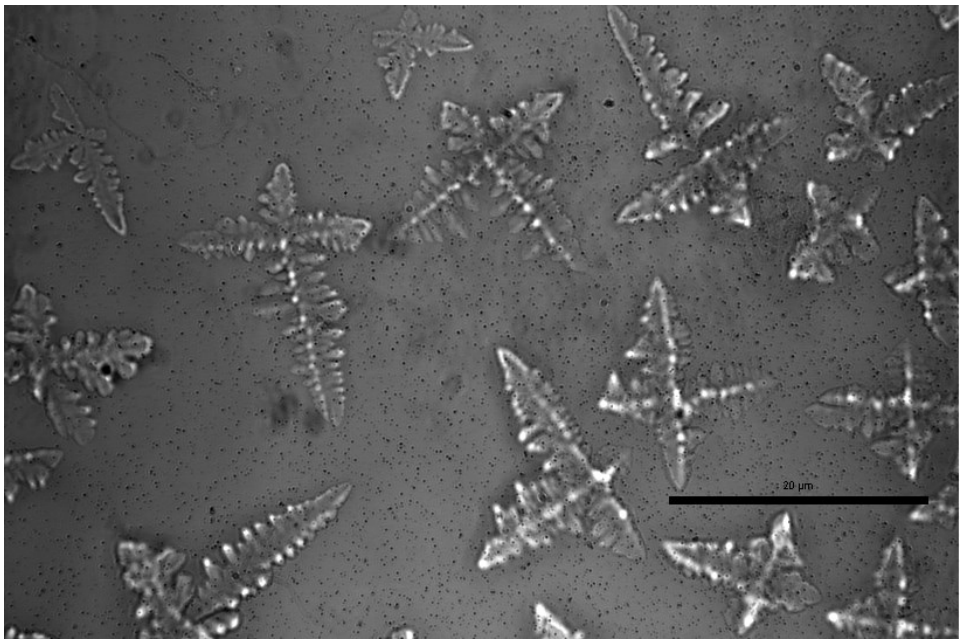

Fig. S8. Experimental images for the proposed models in Fig. 7 in the paper (main text) for (a) m=2, p~1, (b) m=3, p~1.2, and (c) m=6, p~1.6. The scale bar corresponds to 20 µm.

S9. DLVO theory: a theoretical explanation for the effect of variation in citrate concentration

The DLVO theory addresses the interactions between the citrate coated AuNPs. Below we show the interaction curve for citrate stabilized AuNPs generated from the DLVO theory containing the following interaction terms

$V_T = V_D + V_H + V_S$

Where, $V_D = 2\pi e_0 \varepsilon r \varphi^2 \ln\left(1 - e^{-\frac{h}{k^{-1}}}\right)/k_B T$

$V_H = -A_{12} r/12 h k_B T$

where V_S represents the steric interaction due to polymer chains which we neglect here. V_D corresponds to the Debye term representing the charge interaction wherein e_0 is the permittivity of the free space, ε is the dielectric constant, φ is approximated by zeta potential, k_B is the

Boltzmann's constant, h is the inter-particle distance, r is the radius of the nanoparticles, and T is the temperature. V_H is the Hamaker's term corresponding to the van der Waals interactions between the AuNPs wherein A_{12} is the Hamaker constant.

The citrate ions attach to the outer boundary of the AuNPs and give rise to a negative surface charge. We measured the zeta potential of the as-prepared AuNPs (using Horiba Scientific Nano Particle Analyzer SZ-100). When we put the measured value of the zeta potential of -32 mV in the model (which is mentioned in [3] as Nanocoatings models written by Prof. Robert Lee), we obtain the graph shown in Fig. S9(a) for the potential energy. Increasing the value of the zeta potential to -45 mV, we get the graph for the potential energy shown in Fig. S9(b);

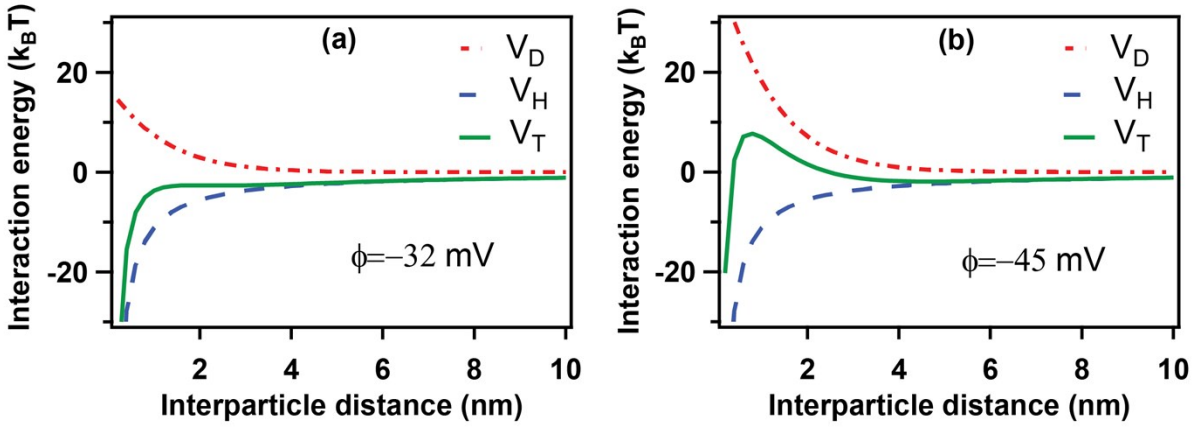

Fig. S9. Interaction energy obtained from DLVO theory for AuNPs having zeta potential of (a) -32 mV and (b) -45 mV.

References

[1] Hunter, Robert J. *Zeta potential in colloid science: principles and applications*. Vol. 2. Academic Press, 2013.

[2] Pamies, R., Cifre, J. G. H., Espín, V. F., Collado-González, M., Baños, F. G. D., & de la Torre, J. G. (2014). Aggregation behaviour of gold nanoparticles in saline aqueous media. *Journal of nanoparticle research*, *16*(4), 2376.

[3] Abbott, Steven, and Nigel Holmes. *Nanocoatings: Principles and Practice: From Research to Production*. DEStech Publications, Inc, 2013.